MedCrave
Step into the World of Research

Journal of Nanomedicine Research

Research Article

Open Access

Effect of Laser Wavelengths on Drug Release with and without Gold Nanoshells and Magnetic Guidance on Uptake by Cancer Cells

Abstract

Liposomes containing Au coated Fe_3O_4 referred to as magnetoplasmonic liposomes (MPL) and doxorubicin (L-Dox) are fabricated to investigate the effects of continuous and pulsed laser wavelengths on drug release from liposomes and magnetic guidance on the uptake of MPL by cancer cell line. Fluorescence microscopy was used to evaluate the apoptosis effect. A maximum temperature of about 6°C was achieved after 400 s for liposomes containing (magnetoplasmonic nanoshells) MPNSs at 100 µg/ml using 514 nm laser. Drug release of almost 100% at saturation point is obtained for MPL-DOX using 532 nm and 514 nm and about 80% and 65% in the case L-DOX for 532 nm and 514 nm lasers, respectively. For cytotoxicity measurement, one control and two treatment groups are studied. The first treatment groups are: with MPNS, with MPL, and laser irradiation. The second treatment groups are: laser hyperthermia using MPL, MPL with magnetic field (MF), MPL-DOX, and MPL-DOX with magnetic field (MF). The pulsed 532 nm laser produced higher cancer cells death i.e., lower viability in comparison to (continuous wave) CW 514 nm laser. Fluorescein isothiocyanate (FITC)-conjugated Annexin-V is used to detect cellular morphological changes at both wavelengths during the apoptosis process due to its ability of binding to phosphatidylserine at the outer surface of plasma membrane. The formulation of MPL-DOX-MF is shown to be a potential system for combined magnetically guided photothermo-chemotherapy of cancer.

Keywords: gold nanoshells, liposome, laser, magnetic guidance, uptake, drug release

Volume 6 Issue 2 - 2017

Mohammad E Khosroshahi,[1,2,3] Lida Ghazanfari,[1,4] and Zahra Hassannejad[1,5]

[1]Laser and Nanobiophotonics Laboratory, Amirkabir University of Technology, Iran

[2]MIS-Electronics, Nanobiophotonics and Biomedical Research Lab, Canada

[3]Department of Mechanical and Industrial Engineering, University of Toronto, Canada

[4]Eshelman School of Pharmacy, University of North Carolina, USA

[5]Sina Trauma and Surgery Research Center, Tehran University Medical Sciences, Iran

Correspondence: Mohammad E Khosroshahi, Laser and Nanobiophotonics Laboratory, Biomaterial Group, Faculty of Biomedical Engineering, Amirkabir University of Technology, Tehran, Iran, Email: khosrom@mie.utoronto.ca

Received: August 17, 2017 | **Published:** September 21, 2017

Introduction

Nanomedicine deals with diagnosis, monitoring and treatment of diseases such as cancer and as well as control and understanding of biological systems. It is generally known that cancer treatment mainly relies on chemotherapy and radiotherapy where most anticancer drugs are essentially taken up by cells with high proliferative rate, a characteristic of cancer cells. However, normal tissue can also suffer from chemotherapeutic action, leading to undesirable side effects. To overcome these issues, strategies such as passive and active targeting have been proposed where they have a key role in nanomedicine for example in innovative controlled drug delivery and release systems that increase the bioavailability and concentration of anticancer drugs at target site.[1,2] Nanomaterials with special designs are frequently used as drug delivery systems to develop highly selective and effective diagnostic and therapeutic modalities.[3,4] Interestingly, external stimuli including electrical and magnetic fields can be utilized to suitably trigger the drug-loaded carriers to release the drug content in a controlled manner.[5]

Basically, liposomes are lipid constituents with hydrophobic head and hydrophilic tail groups and are considered as a potential candidate for delivering the encapsulated nanoparticles (NPs) due to their ability to carry large amount of payload, improved stability, and selective delivery and hence minimizing the NPs side effects such as toxicity. Therefore, the guidance of drug-loaded carriers to specific targets has significant importance in nanomedicine research where less toxic side effects and improved efficiency of therapy are prime goals. In magnetically guided NPs such as liposomes, an external magnetic field is used to transport magnetic NPs loaded with drugs to a specific site within the body or to increase the upload capacity.[6,7] Also, Anderson et al.[8] have shown the feasibility of optically guided controlled release from liposomes containing a molecular load and gold nanoparticles due to nanobubbles. In a research, liposomes contrast agent has been utilized for drug release and photoacoustic imaging applications, which showed these can have better contrast at a depth of about 2-cm.[9] Superparamagnetic iron oxide nanoparticle (SPION) with their significant physicochemical properties such as absence of hysteresis loop, high field irreversibility, high saturation field, extra anisotropy contributions, chemical composition, granulometric uniformity, crystal structure, surface structure, adsorption properties, solubility and low toxicity and, particles size with overall narrow uniform size distribution have made them a serious and reliable candidate for in various fields, such as biomedical applications.[10-12] In magnetically responsive nanoparticles (MNPs), NPs are encapsulated or embedded in a larger colloidal structure that carries a drug. The former approach is more feasible due to the availability of hydrophilic layers, however, in order to produce sufficient temperature increase to destabilize the lipid layer to release the liposome content, large amount of MNPs should be used It is suggested by Liao et al.[13] that Cetuximab-immunomicelles are a useful delivery vehicles for Dox and SPIO to epidermal growth factor receptor overexpressing tumor cells *in-vivo* and that it can serve as MRI-visible and targeted drug delivery. In some applications, MNPs are coated by gold layer to form a gold nanoshell (AuNS) for heating purpose rather than guidance.[14-16] AuNSs are very promising structures, which exhibit unique optical properties such as strong localized surface plasmon resonance (LSPR), surface-enhanced scattering, non-linear optical properties, tunable resonance across the Vis-NIR due to adjustable nanoparticle size and shape.[17-21] Also, due to their inert surface, nontoxicity, surface conjugation chemistry i.e., they can be linked to specific ligands for tumor targeting, imaging and therapies, lack of photobleaching or blinking as with quantum dots, and very low oxidation, AuNSs are considered as biocompatible materials.[22,23] Therefore, they are extensively utilized for cancer diagnostics, imaging and therapeutics.[23,24]

Recently we have demonstrated that Au-coated SPIONs (MPNSs) encapsulated by phospholipid liposomes can be used as exogenous absorber for targeted laser hyperthermia of breast cancer cells.[24] Also, it has been shown by other groups that AuNPs can be conjugated with the anticancer drug Doxorubicin, for drug delivery to liver cancer.[25] When gold nanostructures are irradiated by laser, the absorbed optical energy raises their temperature, hence acting as a localized heat source that is quickly equalized within the nanoparticles. The heat is then transferred to the surrounding environment determined by their thermal relaxation time and laser exposure duration. Therefore, under controlled and optimized conditions drug can be released from thermosensitive liposomes using their light-triggered thermal properties.[26,27] Following our recent reports, here we describe and discuss other parts of research mainly the effect of: (i) continuous wave (CW) and pulsed laser radiation on Dox release from liposomes with and without MPNSs, (ii) static magnetic field on the uptake of MPL by cancer cells, and (iii) the corresponding cellular morphological changes caused by both laser wavelengths during apoptosis.

Materials and methods

Chemicals and reagents

Most chemicals and reagents purchased include Ferric chloride hexahydrate ($FeCl_3.6H_2O$, 99%), ferrous chloride tetrahydrate ($FeCl_2.4H_2O$, 99%), hydrochloric acid (HCl, 37%), sodium hydroxide, chloroform, formaldehyde solution (H_2CO, 37%) absolute ethanol, Triton X-100 and polyvidone 25 are purchased from Merck (USA). Tetrakis (hydroxymethyl), phosphonim chloride (THPC), aqueous solution, Gold (III) chloride trihydrate ($HAuCl_4.3H_2O$, ≥49% Au basis), 3-aminopropyltriethoxysilane (APTES), and Doxorubicin hydrochloride (DOX) are purchased from Sigma-Aldrich (USA). Dipalmitoylphosphatidylcholine (DPPC), cholesterol (Chol), and 1,2-distearoyl-*sn*-glycero-3-phosphoethanolamine-N-.amino(polyethylene glycol)-2000 (ammonium salt) (DSPE-PEG2000) are purchased from Avanti Polar Lipids (USA). MCF-7 cell line is purchased from the Pasteur Institute (Iran). RPMI 1640 medium and fetal bovine serum (FBS) are purchased from GIBCO (USA). Annexin-V-FLUOS staining kit is purchased from Roche (Switzerland). Deionized water (18 MΩ.cm) is provided by a Milli-Q system and deoxygenated by vacuum for 1 hour prior to the use.

Cytotoxicity and uptake

The details of synthesis process are same as those described previously.[27,28]The Step procedure of preparation and application of laser-induced drug release and photothermal apoptosis of cells is illustrated in Figure 1.

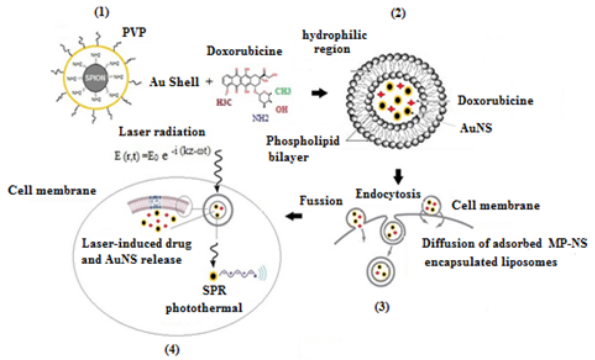

Figure 1 Procedure of preparation and application of the magneto-nanoliposomes: (1) synthesis of MPNS, (2) uptake of MPNS by liposome, (3), (d) endocytosis process, (4) laser-induced drug and MPNS release in cell.

For evaluation of cytotoxicity and hyperthermia experiments, RPMI 1640 medium with 10% FBS was used to cultivate the MCF-7 breast cancer cells and maintained at 37 °C in a 5% CO_2 incubator. For cytotoxicity assay, MTT (3-(4,5-dimethylthiazol-2-yl)-2,5-diphenyltetrazolium bromide) tetrazolium was used. 1×10^4 cells per well were cultivated in 96-well plates overnight as suggested by Kulshrestha.[29] The first group was divided into: the control group (untreated cells), MPNS only, MPL (at a lipid concentration of 10 mM) only, and laser irradiation only. For the control group, the cells were washed with PBS and the fresh cell culture media was then placed in an incubator for the next 24 h. The cells were cultured separately in 200 µl medium containing MPNS and MPL (at lipid concentration of 10 mM), respectively. The culture plates were positioned on the 96-well format magnetic plate (Chemicell-Germany) to study the effect of magnetic field. The cells were then washed after 75 min with PBS and incubated for another 24 h with fresh medium. The second treatment groups included: laser hyperthermia mediated by MPL only, MPL with magnetic field (MF), MPL-DOX only and MPL-DOX with MF, all with a lipid concentration of 10 mM. The *In vitro* hyperthermia of MCF-7 cells incubated with MPL-DOX was done using Argon laser (Melles Griot /43 Series Ion Laser-USA) at 350 mW for 5 minutes with or without Dox. The thermometer was connected to a Windows-based laptop where the results were recorded. The temperature was maintained at 37±0.4 °C recorded by a digital thermometer (Model No. HP-34420A). Since, the drug release from low temperature sensitive liposomes occurs via grain boundary permeabilization when it is heated into the region of its phase transition temperature and the grain boundary structures of the bilayer could bind proteins that are responsible for opsonization, therefore, to reduce the toxicity (by avoiding the opsonization) a few mol % of DSPE-PEG2000 was added to cover the bilayer. *In vitro* evaluation of cellular uptake was based on 15 min incubation of cells in a solution containing Ca^{2+} ions and annexin V-FITC (at a final concentration of 1 µg/mL). The annexin V-binding buffer consists of 10 mM HEPES–NaOH, pH 7.4, 150 mM NaCl, 5 mM KCl, 1 mM $MgCl_2$, and 1.8 mM $CaCl_2$. The stained cells were mounted on slides and immediately visualized under the fluorescence microscope.

Characterization

The characterization process was performed according to flow diagram shown in Figure 2.

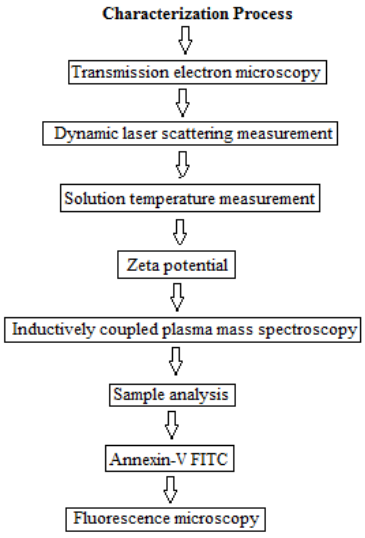

Figure 2 Flow diagram of characterization process.

Transmission electron microscopy (CM 200 FEG STEM Philips-M.E.R.C) operating at 200 kV was used to study liposome samples. The size of nanoparticles determined by TEM is the average of least 50 measurements and reported mean ± standard deviation where SPSS 15.0 was used to perform the calculations. The difference between control and treated groups was compared using paired-sample t-test. P values less than 0.05 are considered to be statistically significant. The mean hydrodynamic radius and polydispersity of the liposomal vesicles were determined by Dynamic Laser Light Scattering (DLS-Malvern). The solution temperature change was measured using a thermistor probe (Redfish Sensors Inc., Model QTGB-14 D3) with an accuracy of 0.15% coupled to a thermometer (Model No. HP-34420A). The output of the thermometer was connected to a Windows-based laptop to read the data. Stability of MPL formulation was evaluated by measuring the zeta potential where it was measured by means of laser microelectrophoresis in a thermostatted cell at room temperature (Brookhaven Instruments Corporation, USA). Every measurement was repeated 5 times and the encapsulation efficiency of AuNSs within the liposomes was determined by inductively coupled plasma mass spectrometry (ICP-MS). Samples for ICP-MS (VARIAN 735-ES) analysis were frozen, lyophilized, and dissolved in nitric acid hydrochloride, prepared by adding nitric acid (100 µL) and hydrochloric acid (300 µL of 37%) for 72 h to dissolve particles. Then, samples were diluted to 2 mL with HNO_3 (1.6 mL of 2%) and analyzed via ICP-MS against standards. Since apoptosis occurs via phospholipidserine transfer from inner surface of cytoplasm to outer surface of cell membrane, Annexin-V FITC agent was used as fluorescent probe which has highest affinity to attach to phospholipidserine and can be observed under fluorescence microscope. The fluorescence microscopy images of MPL-DOX in MCF-7 cells obtained by a fluorescence microscope Eclipse 80i (Nikon, Japan).

Encapsulation efficiency

A value of 54% was obtained for the encapsulation efficiency using the relation (We/Wi)×100 % based on the ICP-MS results where Wi is initial concentration of Fe (mg/mL) in hydration solution and We is encapsulated concentration of Fe (mg/mL) in liposomes. The absorption efficiency of the synthesized MPNS at λ_{SPR} of 531 nm corresponds to 0.656 (AU) where λ_{SPR} represents the surface plasmon resonance wavelength. The efficiency of transformation of absorbed optical energy by MPNS into the thermal energy is given by maximum value of $\Delta T / I$ where T is the temperature and I is constant intensity of laser radiation. In our case, the nanoshell efficiency parameter is found to be 2×10^{-5} °C cm²/W. An efficiency of 95% was calculated for DOX loaded MPL nanoparticles. The liposome formulation DPPC: cholesterol: DSPE-PEG2000 has a melting temperature, T_m of about 41.3 °C.[30] and shows DOX release of less than 5% at 37 °C following 24 h incubation. The release rate of thermosensitive liposome varies according to the composition of liposome, its preparation procedure, and heating temperature.[31] The relation between percentage release and exposure time is found to follow the first-order kinetics expressed as.[32]

$$R(t)\%=R_c(1-e^{-k_{rel}t}) \quad (1)$$

Where % $R(t)$ is the percentage of drug released at exposure time t, k_{rel} is rate of liposome release and R_c is the total percentage of drug released at a given heating temperature.

Results and discussion

Figure 3a represents TEM image of MPNS encapsulated liposomes with an example of sample. The average size of SPIONs and MNPSs are measured 9.5 ± 1.4 nm and 15.8 ± 3.5 nm respectively. TEM of liposome containing DOX only (L-DOX) is seen in Figure 3b and when the liposomes are embedded by MPNS and DOX (MPL-DOX) is shown in Figure 3c.

Figure 4a shows total absorbed power as a function of core and shell diameters at different heat coefficient parameters. Clearly, the variation of total absorbed power geometrically depends on shell diameter rather than core diameter.[21] However, in the case of MPL (Figure 4b), the maximum rise in temperature of about 6°C was obtained when the samples were irradiated by an argon laser at 17 W/cm² for 400 s. These results demonstrate that the temperature increase is sufficient to cause the apoptosis about 42-45 °C. The main factors that influence the value of temperature are MPNS concentration, the laser power and the irradiation time.

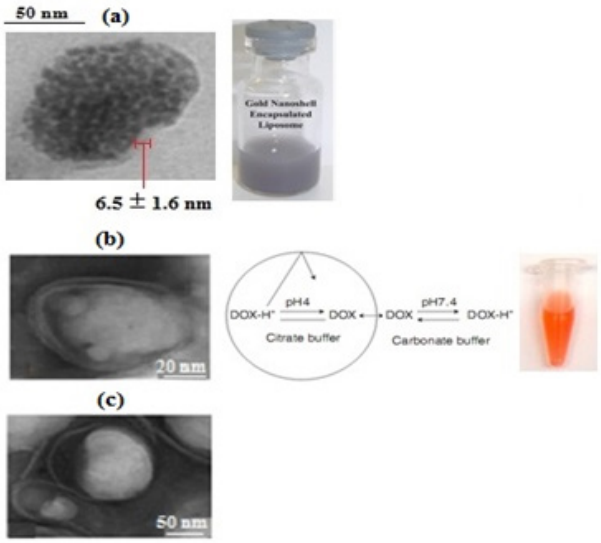

Figure 3 TEM images showing (a) MPNS encapsulated liposome (MPL) with an example of prepared nanoparticles (b) doxorubicin-loaded liposome (L-DOX) with an example of prepared nanoparticles, and (c) DOX and MPNS loaded liposome (MPL-DOX).

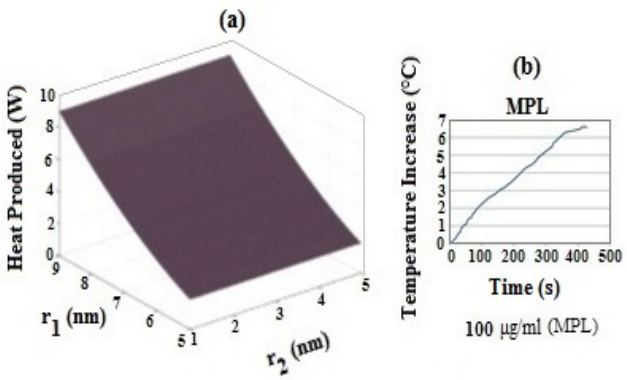

Figure 4 (a) Simulation of total absorbed laser power versus inner and outer radii of MPNS, where r1 and r2 are the inner and outer radii of shell, respectively and (b) temperature increase of MPL with the NP concentration of 100 µg/mL during irradiation by 514 nm Ar laser.

Assuming there is no phase transformations, the temperature distribution around optically-stimulated plasmonic nanoparticles (i.e., heat source) placed in a surrounding medium described by the paraboloic Fourier's heat conduction equation.

$$\rho_g(r)\, c_g(r)\frac{\partial T(r,t)}{\partial t}=K_m\nabla^2T(r,t)+Q_s(r,t) \quad (2)$$

Citation: Khosroshahi ME, Ghazanfari L, Hassannejad Z. Effect of Laser Wavelengths on Drug Release with and without Gold Nanoshells and Magnetic Guidance on Uptake by Cancer Cells. *J Nanomed Res.* 2017;6(2):1–6. DOI: 10.15406/jnmr.2017.06.00152

Where $T(r,t)(K)$ is local temperature, $Q_s(W/m^3)$ is the heating source $\rho_g(r)(Kg/m^3)$, and $c_g(r)(J/K_g K)$, are density, and specific heat of a AuNS, respectively, K_m is the thermal conductivity of the surrounding medium (W/mK), and r is the radius distance (m) from the heated nanoparticles For a single AuNS exposed to a laser beam the power of heat generation is

$$P = I\,\sigma_\alpha \quad (3)$$

where σ_α and I are absorption cross-section and the laser intensity respectively. The total absorbed power by AuNS is.[33]

$$Q = \frac{2\pi Nn|E_{\text{water}}|^2\sqrt{\varepsilon_3}}{15\lambda}.\left(\frac{\varepsilon_2\varepsilon_a-\varepsilon_3\varepsilon_b}{\varepsilon_2\varepsilon_a+2\varepsilon_3\varepsilon_b}\right) \quad (4)$$

where N is the total number of nanoshells, n is real part of refractive index of water (cell), r_1 and r_2 are the radii of SPION core and Au shell respectively, $\varepsilon_a = \varepsilon_1(3-2P) + 2\varepsilon_2 P, \varepsilon_b = \varepsilon_1 P + \varepsilon_2(3-P), P = 1-(r_1/r_2), \varepsilon_1, \varepsilon_2$ and ε_3 are dielectric functions of the core, shell and water respectively. Previously we reported.[21] the simulated results of total absorbed power as a function of core and shell diameters at different heat coefficient parameters. Figure 5a represents the schematic illustration of laser irradiation of AuNS containing liposomes where LSPR-induced photothermal waves cause thermal degradation of liposome membrane which consequently releases the drug.

In the absence of laser, the simplest way for drug release is by diffusion through the lipid bilayer which is maximum when the bilayer is disrupted or undergoes a total phase transition. Therefore, the permeability of the bilayer affects drug diffusion and the permeability of liposomes is considerably increased near the membrane melting temperature.[34] It is also well known that the Zeta potential, which is the electrostatic potential and exists at the shear plane of a particle, is related to both surface charge and the surrounding medium. The electrostatic interaction between nanoparticles and the liposome can influence contributions such as van der Waals interaction and subsequently affecting the length of hydrocarbon chains and also, induces phase separation which results in reduced stability of the vesicles and thus the fluidity.[35,36] The mobility of phospholipids and protein molecules within the membrane increases with the fluidity of bilayer as a result of which some biological functions such as transport or cell signaling are readily achieved.[37]

This can be further enhanced by Zeta potential of Au-coated SPION which possess a negative surface charge, thus causing a notable effect on the phase transition profile of DPPC.[38] Figure 5b compares the rate of drug release for L-DOX and MPN-DOX when irradiated with lasers. There are two points to note (i) the release rate is considerably higher in the case of MPN-DOX, (ii) pulsed laser has been more effective than CW argon laser in trigging the cargo release. Drug release of almost 100% at saturation point was obtained in the case MNP-DOX for both 532 nm and 514 nm, about 80% and 65% in the case L-DOX for 532 nm and 514 nm respectively. The laser exposures were 5 pulses for 532 nm and 5 minutes with 350 mW for 514 nm and 24 h incubation at 37 °C. Following the aforementioned discussion, generally, the rate of liposome membrane fluidity, hence viscosity and the phase transition increases with temperature. In other words, higher the temperature, lower the lipid ordering parameter, i.e., the ratio of the magnetic interaction energy, U, to the Boltzmann thermal energy, kT, where $k = 1.38 \times 10^{-23}$ JK^{-1} is Boltzmann constant and T is temperature, which implies a transition from ordered gel phase to disordered liquid crystalline phase and thus increased membrane permeabilization. Assuming that most biomolecules such as membrane phospholipids and certain types of proteins have a cylindrical structure then.[39]

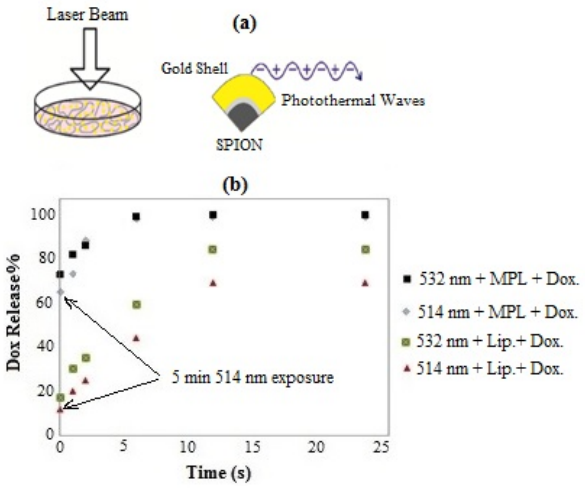

Figure 5 (a) Schematic illustration of laser-induced photothermal waves due to SPR effect causing enhanced drug release and (b) rate of drug release from liposome with and without MPNSs using CW 514 nm and pulsed 532 nm lasers.

$$\frac{U}{kT} = \frac{VB^2(\chi_{||} - \chi_\perp)}{2\mu_0 kT} \quad (7)$$

Where $\mu_0 = 4\pi \times 10^{-7} H \cdot m^{-1}$ is magnetic permeability, V is the molecular volume, B is the magnetic flux density and χ is the difference between magnetic susceptibilities along axes oriented parallel and perpendicular to the long axis of the cylinder. There are various types of molecular assemblies that become oriented when exposed in an aqueous medium to the static magnetic field due to summation of the diamagnetic anisotropies of the individual molecules within assembly it is suggested that drug release from low temperature sensitive liposomes occurs via grain boundary permeabilization when it is heated into the region of its phase transition temperature.[40] However, because the grain boundary structures of the bilayer could bind proteins that are responsible for opsonization, a few mol % of DSPE-PEG2000 is added to cover the bilayer to reduce the toxicity (by avoiding the opsonization).[41] Several mechanisms have been suggested for light-induced membrane destabilization to promote cargo release. These include: light-induced oxidation, photocrosslinking, photoisomerization, photocleavage and photothermal release.[41] In the case of MPN-DOX, photothermal release which is based on the conversion of light into heat is mediated and enhanced due to presence of AuNS and SPR-induced thermal effect, thus more efficient than L-DOX. Also, the reason for higher rate of release in the case of pulsed laser than CW laser can be due to formation of unstable microbubble cavitation generated by each pulse, which grows rapidly followed by its collapse.[42] In a similar experiment, Mathiyazhakan et al.[43] reported that photoresponsive liposomes loaded with AuNPs failed to release calcein upon 514 nm CW laser but successfully released it with an Nd: YAG pulse laser.

Magnetic guidance is one of the strategies for the accumulation of nanoparticles. Therefore, when the magnetic field is applied, most of the MNS are accumulated at the bottom of the wells, where the

cells are present. It is also, known that phospholipid compositions exhibit some changes in turbidity when exposed to static magnetic field at pretransition temperatures.[38] Figure 6 demonstrates the effect of applied magnetic field on uptake of MPNS by MCF 7 cells after 75 minutes incubation.

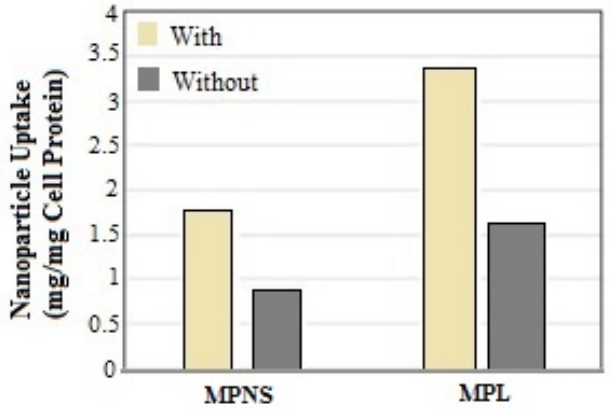

Figure 6 Uptake of MPNS and MPL nanoparticles with nanoshell concentration of 25 μg/mL by MCF 7 cells with and without applied magnetic field (MF).

Clearly, the uptake of MPNS and MPL is higher when magnetic field is applied and that it is significantly higher in MPL case. This can be can be explained in terms of possible higher density number of MPNS encapsulated by liposomes than in unencapsulated case, hence enhanced effect of electrostatic force. In addition, the interaction of liposome-cell should be considered where the liposome charge plays a key role in internalization of nanoparticles either by endocytosis or fusion mechanism. Adsorption of charged particles at the surface of the cell membrane due to strong electrostatic attractions can cause a change in cell morphology and the cell deformation.[44]. Smaller nanoparticles are trapped into bilayer during the interaction process due to membrane flexibility and elasticity thus; the lipid ordering is altered leading to higher degree of fluidity and mass transport. Normally, cationic liposomes bind to cells more easily than anionic liposomes because of their opposite charges.[45] The work required to bring the cell and liposome into contact is defined as the work of adhesion, it is positive for repulsive interaction potentials, and negative for attractive interactions. Therefore, during the contact time the probability of internalization by either the above mechanism is increased.[46] Nanoparticle uptake by cell occurs in two steps i.e., binding of nanoparticles to the cell surface followed by the internalization via for example endocytosis pathway. When nanoparticles bind onto the negatively charged cell surface with the same sign of Zeta potential, the free energy of the ions at a distance from the cell surface increases and $\beta_{binding}$ is positive i.e., the relative zeta potential is $|Z| > 1$, where $\beta(x)$ measures how the presence of nanoparticles affect the free energy of the ions at a distance from the cell surface. However, when $Z\ r <\ 1$ the free energy of the ions at a distance from the cell surface decreases and β binding becomes negative and the internalization mechanism dominates.

It is known that when cells are heated, they develop resistance to heat, which reduces the likelihood of being destroyed by direct thermal cytotoxic effects. Because hyperthermia alters the cell walls via heat shock proteins, cancer cells then react much more effectively to the radiation.[47] Thus, to avoid this effect, the cells are normally preheated prior to laser hyperthermia, which in our case it was done by using a water bath (Lab Companion, USA). The heating effect of surrounding liquid medium on viability of MCF-7 cells was assessed after being heated for 5 min at the temperature of 43 °C. The cytotoxic effects of laser hyperthermia and chemotherapy using the prepared formulation as single and combined modalities are illustrated in Figure 6, where Figure 7a & 7b represent the results for lasers 514 nm and 532 nm respectively. Data are presented as a percentage of the cell viability where viability of control group is taken as 100%. The results are as follows: (i) the viability tests obtained by 532 nm laser are better than 514 nm. This can be explained by the fact that 532 nm wavelength matches with the SPR peak of AuNS where it exhibits the maximum absorption compared with 514 nm. Based on the SPR absorption by AuNS, the energy relaxation is followed through a non-radiative decay channels which results in an increase in kinetic energy, leading to overheating of the local environment around the light-absorbing species. Also, more efficient cell destruction can be achieved by pulsed lasers via microbubble mechanism than CW mode mainly due to shock mechanism, (ii) application of magnetic field produces a better hyperthermia results than without it because it increases the possibility of AuNSs concentration, hence resulting in a stronger localized SPR and thus more efficient photothermal effects, (iii) the MPL-Dox-MF combination at Dox concentrations of 0.5 μg/mL (IC-50 of MCF-7 cells).[47] and 0.1 μg/mL in the case of MPL-Dox produced better viability results i.e., less than 1% and 15% respectively when using 532 nm laser wavelength (Figure 7b) than 514 nm i.e., more cancer cells are damaged. An analysis of these combined treatments using Valeriote's formula.[48] shows that the magnetically targeted MPL-DOX and laser hyperthermia treatments are synergistic in nature.

Figure 8a indicates the results for DOX uptake of 0.13μg/mL concentration by MCF 7 cells seen as red spot (i.e., DOX fluorescence peak) after 75 min and 24 h follow up with relatively higher rate in the latter case (b2), the arrows delineate the spots. The next experiment was to irradiate the MPL samples consisting 25μg/mL of AuNS using 514 nm for five min and 532 nm for 10 pulses and then observe the results after 24 h (Figure 8b). Throughout the experiment, the samples were under magnetic field. As expected, the apoptosis due to photothermal effect is seen as green spots due to annexin-V fluorescence within cell membrane. Clearly, the effect is more dominant when pulsed 532 nm laser was used (b1).

Figure 9 shows MPNS-DOX loaded liposomes are incubated with MCF-7 cells for about 75 min (with and w/o MF) and irradiated with Ar laser at 37 °C. The internalized MPL-DOX in the acidic organelles of MCF-7 cells, which would activate the fluorescence of doxorubicin quenched by Au nanoshells due to nanosurface energy transfer (NSET), demonstrating the presence of NSET between the doxorubicinyl groups and Au nanoshells.[49] Figure 9a demonstrates that the results are more significant when the samples were under direct and continuous influence of external magnetic field where both apoptosis-annexin-V reaction (green) and Dox fluorescence (red) in the area or the nucleus are dominant (a1,a2). The nucleus of the cells in MPL-DOX-w/o MF (b1,b2) does not show this fluorescence. This confirms that under magnetic field, the drug loaded NPs are internalized by the cells. The same experiment was repeated using 532 nm laser and the results shown in (Figure 9b) points out the same conclusion as before except with much stronger significance. It has been reported that chemosensitivity to DOX in MCF7 is due to the decreased level of DNA double-strand break repair proteins, Rad 51.[50] Aroui et al.[51] have shown that the major mechanism of DOX activity is the inhibition of topoisomerase II and stabilization of a ternary drug-topoisomerase II (TOPO II)-DNA complex, causing DNA damage and induction of apoptosis. Furthermore, Prasad et al.[52] have shown that hyperthermia causes apoptosis by irreversibly damaging the

actin and tubulin structures of cells. Other cellular structures such as enzyme complexes, which are required for DNA synthesis and repair, can be damaged by hyperthermia.[53] Recently, Khosroshahi et al.[15] used SPION-based gold and folic acid conjugated nanodendrimers for laser hyperthermia where the formation of cellular crystallization was observed. This was suggested to be due to dehydration where water is vaporized from the cells during laser-induced irradiation, hence leading to a supersaturated solution and mineral such as sugar or salt which precipitate inside the cells. During the dehydration process, the crystals that are formed can damage the cell membrane causing the cell to burst (i.e., a mechanical type of hemolysis) hence leading to cell death. In Figure 9b (a3, b3) membrane exhibits an irregular morphological changes and bulging which are normally identified as characteristic of apoptotic cells, which is a mode of cell death accompanied by specific alterations to the plasma membrane.[54] Redistribution of phosphatidylserine from the inner to the outer plasma membrane leaflet has become one of the most widely used markers for apoptotic cells in mammals. This is largely due to the availability of annexin-V probe, as a sensitive phosphatidylserine-binding protein.

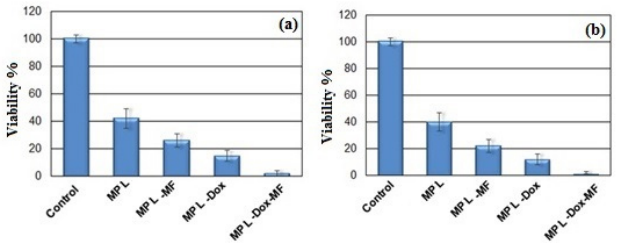

Figure 7 Comparison of cytotoxicity profile of MPL and MPL-DOX formulations on MCF-7 cells (mean ± SD; n=3, P < 0.05) with and without applied MF during the incubation for (a) 514 nm laser and (b) 532 nm laser.

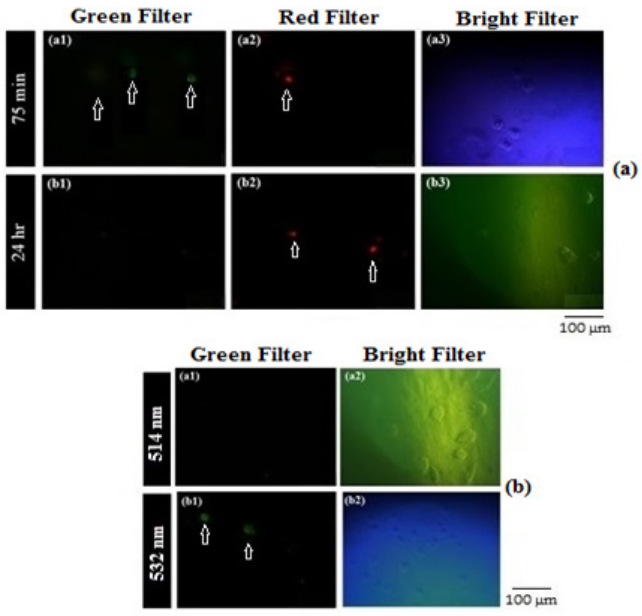

Figure 8 Uptake of L-DOX by MCF-7 cells. The cells are incubated with drug loaded liposomes only for about 75 min and 24 h, (a): (a1-b2) shows the red DOX fluorescence image, (b) apoptosis images of MCF-7 cells after irradiation with 514 nm and 532 nm lasers with stronger effects produced by 532 nm laser (b2). The DOX red fluorescence and apoptosis green fluorescence are indicated by arrow. The images are obtained by the fluorescence microscope equipped with green and red filters for Annexin-V FITC and DOX respectively (n = 3).

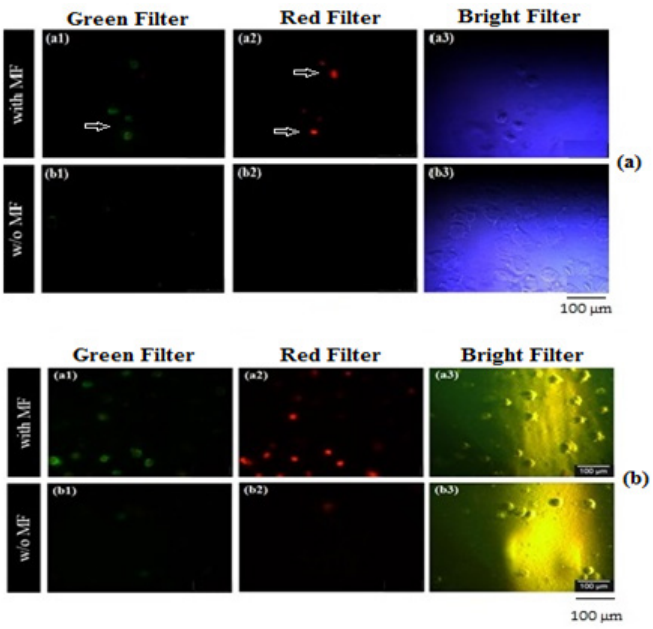

Figure 9 Uptake of MPL-DOX by MCF-7 cells. The cells are incubated with drug loaded MPL for about 75 min, (a): (a1-a3) with MF, (b1-b3) without MF and irradiated with 514 nm laser at 37°C, (b) same as above using 532 nm laser. The DOX red fluorescence and apoptosis green fluorescence are indicated by arrow. The images are obtained by the fluorescence microscope equipped with green and red filters for Annexin-V FITC and DOX respectively (n = 3).

Conclusion

The cytotoxicity, uptake, combined effects of laser-induced hyperthermia and drug release of the formulation of MPL-DOX are studied at presence and absence of magnetic field. The pulsed 532 nm laser produced higher cancer cells death i.e., lower viability in comparison to CW 514 nm laser. The FITC-conjugated annexin V-binding assay using fluorescence microscopy provided a specific and rapid imaging technique to detect apoptosis. The enhanced uptake of DOX under magnetic field was confirmed. We believe the formulation of MPL-DOX-MF can be used as potential system for combined magnetically guided photothermo-chemotherapy of cancer, particularly using pulsed or modulated NIR lasers to avoid undesirable photothermal damage to surrounding healthy cells.

Conflicts of interest

The authors declare no conflict of interest.

References

1. Lammers T, Hennik W, Storm G. Tumour–targeted nanomedicines: principles and practice. *Br Cancer*. 2008;99:392–397.
2. Allen T. Ligand–targetedtherapeutics in anticancer therapy. *Nat Rev Cancer*. 2002;2(10):750–763.
3. Puvvada N. Nanomedical platform for drug delivery. *J Nanomed Nanotech*. 2011;2:1–5.
4. Yiv S, Uckun F. Lipid spheres as attractive nanoscale drug delivery platforms for cancer therapy. *J Nanomed Nanotechnol.* 2012;3:1–6.
5. Kaushik A, Jayant R, Sagar V. The potential of magneto–electric nanocarriers for drug delivery. *Expert Opin Del*. 2014;11(10):1635–1646.
6. Kuznetsov AA, Filipov VI, Alyautdin RN, et al. Application of magnetic liposomes for magnetically guided transport of muscle relaxants and anti–cancer photodynamic drugs. *J Mag Mat.* 2001;225:95–100.

7. Lee J, Ivkov R, Blumenthal R. Magnetically triggered drug release from liposome embedded Gel. *J Nanomed Biotherapeutic.* 2014;4:1–6.

8. Anderson L, Hansen E, Lukianova–Hleb EY, et al. Optically guided controlled release liposomes with tunable plasmonic nanobubbles. *J Cont Rel*. 2010;144(2):151–158.

9. Sivasubramanian K, Mathiyazhakan M, Wiraja C, et al. Near–infrared light responsive liposomal contrast agaent for photoacoustic imaging and drug release applications. *J Biomed Opt*. 2017;22(4):041007.

10. Pankhurst Q, Thanh N, Jons S, et al. Progress in applications of magnetic nanoparticles in biomedicine. *J Phys D Appl Phys*. 2009;42(22):224001.

11. Jiang Q, Lang QX. Size dependence of structures and properties of materials. *Open Nanosci J*. 2007;1: 32–59.

12. Khosroshahi ME, Ghazanfari L. Preparation and characterization of silica–coated iron–oxide bionanoparticles under N2 gas. *Physica E*. 2010;42:1824–1829.

13. Liao C, Sun Q, Shen J, et al. Targeting EGFR–overexpressing tumor cells using Cetuximab–immunomicelles loaded with doxorubicine and superparamagnetic iron oxide. *Euro Radiol*. 2011;80(3):699–705.

14. Tajabadi M, Khosroshahi ME, Bonakdar S. Imaging and Therapeutic Applications of Optical and Thermal Response of SPION–Based Third Generation Plasmonic Nanodendrimers. *Opt Photo J*. 2015;5:212–226.

15. Khosroshahi ME, Tajabadi M. Multifunctional Nanoplatform for Targeted Laser–induced Hyperthermia and Microscopy of Breast Cancer Cells using SPION–based Gold and Folic Acid Conjugated Nanodendrimers: An *in vitro* Assay. *J Nanomed Nanotech*. 2017;8:1–11.

16. Park SE, Lee J, Lee T, et al. Comparative hyperthermia effects of silica–gold nanoshells with different surface coverage of gold clusters on epithelial tumor cells. *Int J Nanomedicine*. 2015;10:261–271.

17. Pustovalov V, Babenkov V. Optical properties of gold nanoparticles at laser radiation wavelengths for laser applications in nanotechnology and medicine. *Laser Phys Lett*. 2004;1(10):516–520.

18. Khosroshahi ME, Ghazanfari L. Physicochemical characterization of Fe_3O_4/SiO_2/Au multilayer nanostructure. *Mater Chem Phys*. 2012;133(1):55–62.

19. Baffou G, Quidant R. Thermo–plasmonics: using metallic nanostructures as nano–sources of heat. *Laser Photonics Rev.* 2013;7:171–187.

20. Hasannejad Z, Khosroshahi ME. Synthesis and evaluation of time dependent properties of plasmonic–magnetic nanoparticles. *Opt Mat*. 2013;35(3):644–651.

21. Ghazanfari L, Khosroshahi ME. Simulation and experimental results of optical and thermal modeling of gold nanoshells. *Mat Sci Eng C*. 2014;42:185–191.

22. Khlebtsov B, Zharov V, Melikov A, et al. Optical amplification of photothermal therapy with gold nanoparticles and nanoshells. *Nanotechology*. 2006;17:5167–5179.

23. Huang X, Jain PK, El–Sayed IH, et al. Gold nanoparticles: interesting optical properties and recent applications in cancer diagnostics and therapy. *Nanomed*. 2007;2(5):681–693.

24. Khosroshahi ME, Hassannejad Z, Firouzi M, et al. Nanoshell–mediated targeted photothermal therapy of HER2 human breast cancer cells using pulsed and continuous wave lasers: an *in–vitro* study. *Lasers Med Sci.* 2015;30(7):1913–1922.

25. Syed A, Raja R, Kundu G, et al. Extracellular biosynthesis of monodispersed gold nanoparticles, their characterization, cytotoxicity assay, biodistribution and conjugation with the anticancer drug doxorubicin. *J Nanomed Nanotechol*. 2013;4:1–6.

26. Paasonen L, Sipilä T, Subrizi A, et al. Gold embedded photosensitive liposomes for drug delivery: triggering mechanism and intracellular release. *J Control Release*. 2010;147(1):136–143.

27. Khosroshahi ME, Ghazanfari L, Hassannejad Z, et al. *In–vitro* Application of Doxorubicin Loaded Magnetoplasmonic Thermosensitive Liposomes for Laser Hyperthermia and Chemotherapy of Breast Cancer. *Int J Nanomed Nanotech*. 2015;6:1–11.

28. Hassannejad Z, Khosroshahi ME, Firouzi M. Fabrication and characterization of magnetoplasmonic liposome carriers. *Nanosci Technol Symbiosis*. 2014;1:1–9.

29. Kulshrestha P, Gogoi M, Bahadur D, et al. *In vitro* application of paclitaxel loaded magnetoliposomes for combined chemotherapy and hyperthermia. *Colloids and Surfaces B: Biointerfaces*. 2012;96:1–7.

30. Pradhan P, Giri J, Rieken F, et al. Targeted temperature sensitive magnetic liposomes for thermo–chemotherapy. *J Control Release*. 2010;142(1):108–121.

31. Yatvin MB, Mühlensiepen H, Porschen W, et al. Selective delivery of liposome–associated cis–dichloro–diammine–platinum (II) by heat and its influence on tumor drug uptake and growth. *Cancer Res.* 1981;41(5):1602–1607.

32. Woo J, Chiu G, Karlsson G, et al. Use of a passive equilibration methodology to encapsulate cisplatin into preformed thermosensitive liposomes. *Int J Pharm*. 2008;349(1–2):38–46.

33. Pustovalov V, Astafyeva L, Jean B. Computer modeling of the optical properties and heating of spherical gold and silica–gold nanoparticles for laser combined imaging and photothermal treatment. *Nanotechnology*. 2009;20(22):1–11.

34. Yatvin MB, Weinstein JN, Dennis WH, et al. Design of liposomes for enhanced local release of drugs by hyperthermia. *Science*. 1978;202(4374):1290–1293.

35. Wang B, Zhang L, Bae S, et al. Nanoparticle–induced surface reconstruction of phospholipid membranes. *Proc Natl Acad Sci*. 2008;105(47):18171–18175.

36. Bhandary S, Sultana P, Basu R, et al. A study on the modulation of the phase behavior of lipid aggregates–effect of some metal nanoparticles. *Adv Sci Eng Med*. 2011;3(3):213–218.

37. Park S, Oh S, Mun J. Effects of silver NPs on the fluidity of bilayer in phospholipid liposome. *Colloids Surf B*. 2005;44(2–3):117–122.

38. Goertz MP, Goyal N, Bunker B, et al. Substrate effects on interactions of lipid bilayer assemblies with bound nanoparticles. *J colloid Interf Sci*. 2011;358:635–638.

39. Liburdy RP, Tenforde TS, Magin RL. Magnetic field–induced drug permeability in liposome vesicles. *Radiat Res*. 1986;108(1):102–111.

40. Landon CD, Park J, Needham D, et al. Nanoscale drug delivery and hyperthermia: the materials design and preclinical and clinical testing of low temperature–sensitive liposomes used in combination with mild hyperthermia in the treatment of local cancer. *The Open Nanomed J*. 2011;3:38–64.

41. Leung S, Romanowski M. Light–activated content release from liposomes. *Theranostics*. 2012;2(10):1020–1036.

42. Dyer PE, Khosroshahi ME, Tuft SJ. Studies of Laser–Induced Cavitation and Tissue Ablation in Saline using a Fibre–Delivered Pulsed HF Laser. *Appl Phys B*. 1993;56:84–93.

43. Mathiyazhakan M, Yang Y, Liu Y, et al. Non–invasive controlled release from gold Nanoparticle integrated photosensitive liposomes through pulse laser induced microbubble cavitation. *Colloids Surf B*. 2015;126: 569–574.

44. Hayden S, Zhao G, Saha K, et al. Aggregation and interaction of cationic NPs on the bacterial surfaces. *J Am Chem Soc*. 2012;134(16):6920–6923.

45. Allen TM, Austin G, Lin A, et al. Uptake of liposomes by cultured mouse bone marrow macrophages: influence of liposome composition and size. *Biochim Biophys Acta*. 1991;1061(1):56–64.

46. Israelachvili JN. Intemolecuar and Surface Forces: With Applications to Colloidal and Biological Systems. (3rd edn), Academic Press, UK 1985.

47. Osman A, Bayoumi H, Al Harthi S, et al. Modulation of Doxorubicin cytotoxicity by resveratrol in a human breast cancer cell line. *Cancer Cell Int*. 2012;12(1):47.

48. Valeriote F, Lin H. Synergistic interaction of anticancer agents: a cellular perspective. *Cancer Chemother Rep*. 1975;59(5):895–900.

49. Wang F, Wang Y, Dou S, et al.Doxorubicin–tethered responsive gold nanoparticles facilitate intracellular drug delivery for overcoming multidrug resistance in cancer cells. *ACS Nano*. 2011;5:3679–3692.

50. Koehn H, Magan N, Isaacs RJ, et al. Differential regulation of DNA repair protein Rad 51 in human tumour cell lines exposed to doxorubicin. *Anticancer Drug*. 2007;18:419–425.

51. Aroui S, Brahim S, Waard M, et al. Cytotoxicity, intracellular distribution and uptake of doxorubicin and doxorubicin coupled to cell–penetrating peptides in different cell lines: A comparative study. *Biochem Biophys Res Commun*. 2010;391(1):419–425.

52. Prasad N, Rathinasamy K, Panda D, et al. Mechanism of cell death induced by magnetic hyperthermia with nanoparticles of γ–$MnxFe_2$–xO_3 synthesized by a single step process. *J Mater Chem*. 2007;17:5042–5051.

53. George KC, Singh B. Synergism of chlorpromazine and hyperthermia in two mouse solid tumours. *Br J Cancer*. 1982;45(2):309–313.

54. Massart C, Barbet R, Genetet N, et al. Doxorubicin induces Fas–mediated apoptosis in human thyroid carcinoma cells. *Thyroid*. 2004;14(4):1–11.

Citation: Khosroshahi ME, Ghazanfari L, Hassannejad Z. Effect of Laser Wavelengths on Drug Release with and without Gold Nanoshells and Magnetic Guidance on Uptake by Cancer Cells. *J Nanomed Res*. 2017;6(2):1–6. DOI: 10.15406/jnmr.2017.06.00152